

Online Research @ Cardiff

This is an Open Access document downloaded from ORCA, Cardiff University's institutional repository: <https://orca.cardiff.ac.uk/id/eprint/141783/>

This is the author's version of a work that was submitted to / accepted for publication.

Citation for final published version:

Aryal, Nanda and Jones, Owen ORCID: <https://orcid.org/0000-0002-7300-5510>
2021. Spatial-temporal rainfall models based on Poisson cluster processes. Stochastic Environmental Research and Risk Assessment 35 , pp. 2629-2643. 10.1007/s00477-021-02046-5 file

Publishers page: <http://dx.doi.org/10.1007/s00477-021-02046-5>
<<http://dx.doi.org/10.1007/s00477-021-02046-5>>

Please note:

Changes made as a result of publishing processes such as copy-editing, formatting and page numbers may not be reflected in this version. For the definitive version of this publication, please refer to the published source. You are advised to consult the publisher's version if you wish to cite this paper.

This version is being made available in accordance with publisher policies.

See

<http://orca.cf.ac.uk/policies.html> for usage policies. Copyright and moral rights for publications made available in ORCA are retained by the copyright holders.



Spatial-temporal rainfall models based on Poisson cluster processes

Nanda R. Aryal · Owen D. Jones

Received: date / Accepted: date

Abstract We fit stochastic spatial-temporal models to high-resolution rainfall radar data using Approximate Bayesian Computation (ABC). We consider models constructed from cluster point-processes, starting with the model of Cox, Isham and Northrop, which is the current state of the art. We then generalise this model to allow for more realistic rainfall intensity gradients and for a richer covariance structure that can capture negative correlation between the intensity and size of localised rain cells.

The use of ABC is of central importance, as it is not possible to fit models of this complexity using previous approaches. We also introduce the use of Simulated Method of Moments (SMM) to initialise the ABC fit.

Keywords Rainfall; spatial-temporal; spatiotemporal; Approximate Bayesian Computation.

1 Introduction

Our interest in spatial-temporal rainfall models comes from the use of rainfall simulators to understand the responses of hydrological systems to rainfall events. It has been argued by many authors (for example Wheeler et al. [26], Segond et al. [22], Chander et al. [6]) that using simulated rainfall with realistic spatial and temporal variation is an effective way of understanding the range and frequency of responses from any given hydrological system. In particular, extreme responses such as flash floods and debris flows are regularly triggered by storm cells with an area of 4 km^2 and a duration of 30 minutes [10], so we want our models to have this level of detail.

Spatial-temporal rainfall models can typically be broken down into two main parts: a model for the frequency, duration and extent of rainfall events, and a separate model for the spatial and temporal structure of a single event.

31 There is no precise definition of what constitutes a rainfall event, and in prac-
 32 tice it is somewhat model dependent. A rainfall event will not in general exhibit
 33 rainfall contiguous in space and time, but formally we imagine that during an
 34 event any point in space will be rained on more often than not. Within an
 35 event we do see contiguous convex patches of rain which we call rain cells. In
 36 this paper our rainfall events have a timescale of hours and a spatial scale of
 37 thousands of km^2 ; we required that during an event at least 20% of the area
 38 of interest should be receiving rain at any given time.

39 We will concern ourselves solely with models for a single event, for which
 40 we consider stochastic cluster-type models. These models are constructed to
 41 mimic the cell-like structure of rainfall events, and are straight-forward to
 42 simulate. We start with the model of Cox & Isham [7] as extended by Northrop
 43 [15], which we call the CIN model, and then introduce a number of extensions.
 44 The CIN model and our extensions of it are all stationary models for the
 45 interior of a rainfall event; definitions are given in Section 2. To fit them we
 46 use high-resolution rainfall radar data, which gives rainfall intensity on a $1 km^2$
 47 grid every 6 minutes. In what follows we use a single rainfall event covering an
 48 area of $180 \times 180 km^2$ for a duration of 4 hours, described below. The thesis
 49 of Aryal [2] considers other rainfall events at the same and different locations
 50 and obtains similar results.

51 The CIN model assumes that rain cells have constant intensity and does not
 52 allow dependence between the intensity and size of a cell. Our first extension—
 53 the CIN-1 model—incorporates more realistic rainfall intensity gradients and
 54 gives a quantitatively better fit. This mirrors recent results for point rainfall
 55 models [17]. Our second extension—the CIN-2 model—is designed to capture
 56 the negative correlation between the intensity and size of localised rain cells
 57 that has previously been observed in point rainfall models [11]. The results here
 58 are mixed, with moderate evidence of the negative correlation but without a
 59 better fit overall. The implications of this are discussed in the Conclusions
 60 section.

61 Because it has an intractable likelihood function, in the past the CIN model
 62 has been fitted using the Generalized Method of Moments (GMM) [26]. GMM
 63 fitting matches theoretical and observed moments of the process, and thus is
 64 restricted to moments for which you have an analytic expression. However we
 65 do not have analytic expressions for the moments of our extended processes, so
 66 GMM fitting is no longer an option and we instead use Approximate Bayesian
 67 Computation (ABC). ABC fitting compares the observed process to simula-
 68 tions, and places no restrictions on the statistics used to compare them. It
 69 also has the advantage of providing credible intervals for the estimated par-
 70 ameters. We give a brief description of ABC in Section 3, before dealing with
 71 the specifics of the case in hand. In [3] the authors give a comparison of GMM
 72 and ABC fitting for the Bartlett-Lewis point rainfall model, demonstrating
 73 the advantages of ABC.

74 There is an extensive literature on modelling and simulating rainfall at a
 75 single point. In particular there are many models based on cluster point pro-
 76 cesses, going back to the rectangular pulse model of Rodriguez-Iturbe, Cox and

77 Isham [21]. The CIN model that we start with is a natural spatial-temporal ex-
78 tension of these models, and is the most sophisticated spatial-temporal model
79 of this type to have appeared in the literature to date. The surveys of Onof et
80 al. [16] and Wheeler et al. [25] provide a good summary of the current state
81 of the art for these models.

82 There are two main alternative approaches to spatial-temporal rainfall
83 modelling. The first, dating back to Le Clerc and Schaake [12], is to extend
84 point models into space using techniques such as the depth area reduction
85 factor (DARF). These approaches are often used to simulate a single extreme
86 rainfall event, but by their construction they ignore the internal spatial struc-
87 ture.

88 The second alternative is to use random fields rather than cluster processes.
89 Such models do capture the spatial structure of a rainfall event though lack
90 the physical intuition of processes built from cluster point processes. Recent
91 examples of this type of model can be found in the papers of Paschalis et al.
92 [18] and Benoit et al. [5]. These types of model have also been successfully
93 incorporated into more general weather generators [1, 19].

94 The data

95 The CIN model and our generalisations are stationary and are used to model
96 the “interior” of a rainfall event. We will suppose that we have observations
97 of the rainfall in some finite space-time window $A \times [0, T]$, where T is chosen
98 so that the leading and trailing edges of the rainfall event are not observed.
99 For this study we used radar data collected at Laverton, Melbourne, on 24th
100 September 2016 from 12:54 to 16:48 hours, calibrated by the Australian Bureau
101 of Meteorology using rain-gauge data. The data gives rainfall depth in $10^{-2}mm$
102 averaged over $1 km^2$ pixels every 6 minutes for a period of 4 hours. The radar
103 covers a circular region of $128 km$ radius, but we restrict ourselves to a square
104 study area of size $180 \times 180 km^2$. To reduce the noise in the data, rainfall
105 depths of less than $0.01 mm$ for a six minute interval are rounded down to 0.

106 A contour plot of the spatial rainfall intensity at a single time-point is
107 given in Figure 1(a). Looking at the spatial maximum and mean over the
108 study period, and the percentage of the study area covered by rain (Figure
109 1(b-d)), it is reasonable to consider this space-time region as being in the
110 interior of a rainfall event.

111 2 The Cox-Isham-Northrop model and extensions

112 The Cox-Isham-Northrop (CIN) rainfall model is a spatial-temporal stochastic
113 model for a rainfall event, constructed using a cluster point process. The cluster
114 process is constructed by taking a primary point process, called the storm
115 arrival process, and then attaching to each storm center a finite secondary
116 point process, called a cell process. To each cell center we then attach a rain

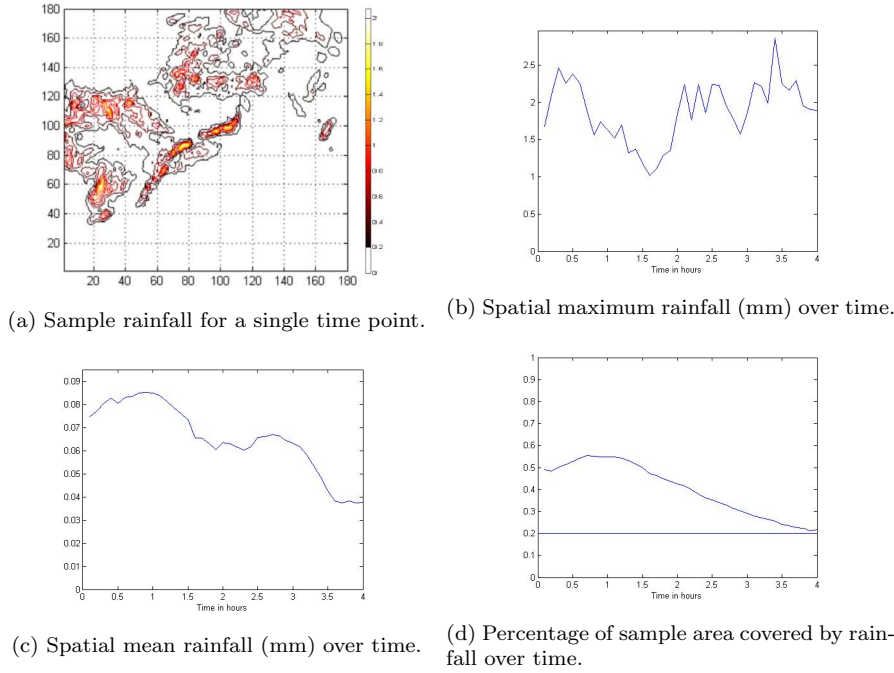


Fig. 1: Rainfall on 24th September 201 from 12:54 to 16:48 hours at Laverton, Melbourne.

117 cell, with an associated area, duration and intensity. The storm and cell centers
 118 all share a common velocity. The total rainfall intensity at point (x, y) and time
 119 t is then the sum of the intensity at (x, y) of all cells active at time t [7, 15].

120 The storm arrival process is taken to be a Poisson process in $\mathbb{R}^2 \times [0, \infty)$
 121 with homogeneous rate λ_s . Let $\mathbf{v} = (v_x, v_y)$ be the velocity of the rainfall
 122 event, so if a storm center arrives at (\mathbf{u}, s) then at time $s + t$ it will be at
 123 $(\mathbf{u} + t\mathbf{v}, s + t)$. Storm durations are random with an $\exp(\gamma_s)$ distribution.

124 While a storm is active it produces cells at a rate λ_c in time, starting
 125 with a cell at the moment the storm begins. If the storm arrives at (\mathbf{u}, s) and
 126 produces a cell at time $s + t$, the cell will be centered at $\mathbf{u} + t\mathbf{v} + \mathbf{w}$, where \mathbf{w}
 127 comes from a Gaussian distribution with mean $\mathbf{0}$ and covariance Σ . The cell
 128 centre then also moves with velocity \mathbf{v} . We parameterise Σ using the storm
 129 diameter d_s , eccentricity e and orientation ω . d_s^{-1} has a gamma distribution
 130 with mean μ_{1/d_s} and coefficient of variation CV_{1/d_s} .

131 Individual cells have random durations, distributed as $\exp(\gamma_c)$, and ran-
 132 dom diameters d_c (the major axis). Rain cells are elliptical, with the same
 133 eccentricity e and orientation ω as the storms. d_c^{-1} has a gamma distribution
 134 with mean μ_{1/d_c} and coefficient of variation CV_{1/d_c} . It is convenient to use

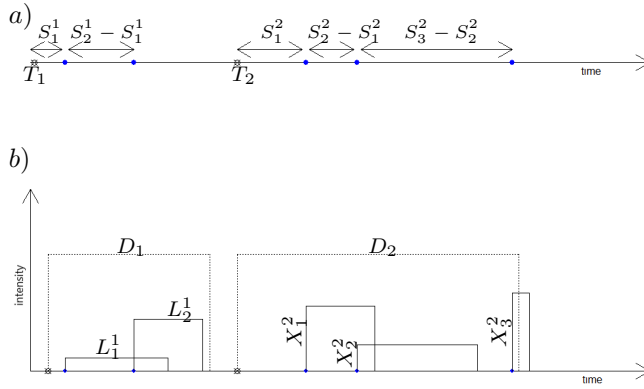


Fig. 2: Schematic of the temporal structure of the CIN model: a) Storm process (storm origins at T_i) and cell processes (the solid points show cell origins). The S_i^j note the times from the storm origins to cell origins; b) Storm durations D_i , cell durations L_i^j , and cell intensities X_i^j .

135 μ_A , the expected area of a rain cell, instead of CV_{1/d_c} , where

$$\mu_A = \pi \sqrt{1 - e^2} \mu_{1/d_c} (1 + CV_{1/d_c}^{-2}).$$

136 For the CIN model the intensity of a rain cell is constant over the area
 137 and duration of the cell, with an exponential distribution mean μ_X . The dis-
 138 placement, duration, diameter, and intensity of a cell are all independent, and
 139 independent of other cells. We give a schematic of the temporal structure of
 140 the CIN model in Figure 2 and of the spatial structure in Figure 3.

141 All together the CIN model has 13 parameters: velocity $\mathbf{v} = (v_x, v_y)$; ec-
 142 centricity e ; orientation ω ; storm rate λ_s ; mean storm duration $1/\gamma_s$; storm
 143 diameter given by μ_{1/d_s} and CV_{1/d_s} ; cell rate λ_c ; mean cell duration $1/\gamma_c$; cell
 144 diameter given by μ_{1/d_c} and μ_A ; and mean cell intensity μ_X .

145 Generalisations of the CIN model

146 To date the CIN model has been the most detailed spatial-temporal rainfall
 147 model available using a stochastic cluster process construction. This is not
 148 because of a lack of scientific imagination, but because of the difficulty in
 149 obtaining theoretical moment expressions for these types of models, which
 150 have in the past been required for model fitting. We present here two novel
 151 extensions of the CIN model, incorporating increased flexibility and realism.
 152 We extend the model in two stages; in both cases the temporal structure of
 153 the process is unchanged and we refine the spatial structure of the rain cells.

154 The first stage we call the CIN-1 model; we incorporate two changes to
 155 give more realistic rainfall intensity gradients and provide a better match with

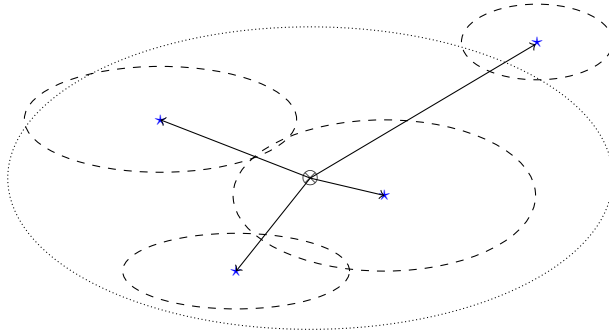


Fig. 3: Schematic diagram of the spatial structure of the CIN model. The centre point is a storm centre (which has a constant velocity). Stars are cell centres and the lines indicate the displacement of cell centres from the storm centre. The dashed curves indicate the cell areas, and the dotted curve gives a 95% prediction region for the storm area.

156 observations. Firstly we suppose that the rainfall intensity decreases continu-
 157 ously from the centre of a cell to the edge, rather than acting as a step function.
 158 If a and b are the lengths of the semi-major and semi-minor axis of a rain cell,
 159 and X is the intensity at the cell centre (c_x, c_y) , then we model the intensity
 160 at (x, y) as

$$X \sqrt{1 - \frac{(x - c_x)^2}{a^2} - \frac{(y - c_y)^2}{b^2}}.$$

161 Secondly we seek to capture an observed variation in the eccentricity of the
 162 cells: some cells appear circular in shape while some are long and thin. Accord-
 163 ingly we suppose that cell eccentricity has a normal distribution with mean
 164 μ_e and variance σ_e^2 , truncated to $[0, 1]$.

165 For the second stage CIN-2 model we introduce correlation between cell
 166 intensity and diameter, again reflecting observed behaviour [11]. Specifically,
 167 for cell intensity X and cell diameter d_c , we suppose that

$$\log \begin{pmatrix} X \\ d_c \end{pmatrix} \sim N \left(\begin{pmatrix} \mu_X \\ \mu_{d_c} \end{pmatrix}, \begin{pmatrix} \sigma_X^2 & \rho_{X,d_c} \sigma_X \sigma_{d_c} \\ \rho_{X,d_c} \sigma_X \sigma_{d_c} & \sigma_{d_c}^2 \end{pmatrix} \right).$$

168 Figure 4 represents the intensity of a single cell in (a) the CIN model and
 169 (b) the CIN-1 and CIN-2 models.

170 3 Model Fitting Using ABC

171 The CIN model has an intractable likelihood: calculating the rainfall intensity
 172 at any given point requires integration over all configurations of the underly-
 173 ing cluster point-process, which is impractical. Thus likelihood-based model
 174 fitting—such as maximum likelihood or Bayesian MCMC methods—can not be
 175 used. Moreover, for spatial-temporal data classical likelihood-free approaches

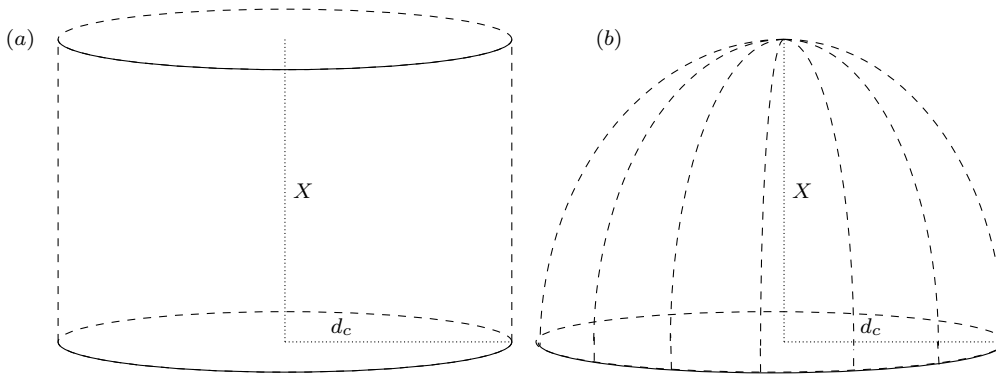


Fig. 4: Cell intensities for (a) CIN model (b) CIN-1 and CIN-2 models.

176 using ranks, permutations or bootstrapping also don't work. Wheeler et al. [26]
 177 successfully used the Generalised Method of Moments (GMM) to fit the CIN
 178 model. However GMM requires analytical expressions for various moments
 179 and in this case their derivation relies on the strong independence assump-
 180 tions present in the CIN model, so this approach does not carry over to the
 181 CIN-1 and CIN-2 models.

182 Simulation based model fitting has been increasing in popularity since the
 183 late 1980's, mirroring the increase in desktop computing power. The Simulated
 184 Method of Moments (SMM) of McFadden [14] uses simulation to estimate
 185 moments which are then compared to observed moments much like GMM, and
 186 can be used to fit the CIN-1 and CIN-2 models (see Gouriéroux and Monfort
 187 1993 [8] for a review of SMM). However SMM is limited in that it only provides
 188 point estimates and does not allow model comparisons, so we only use it to
 189 provide initial estimates for our ABC procedure (details are given below). For
 190 estimation problems with a small number of parameters (not the case here)
 191 we can combine simulation with kernel density estimation to estimate the
 192 likelihood and hence obtain approximate maximum likelihood estimates (see
 193 for example Jones 2007 [9]). Alternatively the synthetic likelihood approach
 194 of Wood 2010 [27] is a more widely applicable method that uses simulation
 195 to form a Gaussian approximation to the likelihood, allowing likelihood-based
 196 inference. Rather than synthetic likelihood we have opted to use Approximate
 197 Bayesian Computation (ABC), which avoids any questions about whether it
 198 is appropriate to use a Gaussian approximation, and has all the benefits of
 199 Bayesian inference. ABC has already been successfully applied in many fields,
 200 but this is its first application to a spatial-temporal rainfall model.

201 ABC is a likelihood-free Bayesian inference technique, which uses simula-
 202 tions from the likelihood of interest in the absence of an analytic form. The
 203 technique developed from numerically intensive techniques for estimating pop-
 204 ulation genetics models [20], and has since seen steadily increasing use in a
 205 variety of applications. The recent collection edited by Sisson, Fan and Beau-
 206 mont [24] gives a comprehensive introduction to the subject. In what follows

207 we use ABC-MCMC, introduced by Marjoram et al. [13], which uses Markov
 208 Chain Monte Carlo to speed up the effective sampling rate of vanilla ABC.

209 We suppose that we have an observation D from some model $f(\cdot|\boldsymbol{\theta})$, de-
 210 pending on parameters $\boldsymbol{\theta}$, and that we are able to simulate from f (so $f(\cdot|\boldsymbol{\theta})$
 211 is the likelihood). Let π be the prior distribution for $\boldsymbol{\theta}$ and $S = S(D)$ a vector of
 212 summary statistics for D , then ABC generates samples from $f(\boldsymbol{\theta}|\rho(S(D^*), S(D)) <$
 213 $\epsilon)$, where $D^* \sim f(\cdot|\boldsymbol{\theta})$, $\boldsymbol{\theta} \sim \pi$, and ρ is some distance function. If S is a suf-
 214 ficient statistic, then as $\epsilon \rightarrow 0$ this will converge to the posterior $f(\boldsymbol{\theta}|D)$.
 215 ABC-MCMC adds a proposal chain with density q and an additional rejection
 216 step, to generate a sample $\{\boldsymbol{\theta}_i\}$. Let $\boldsymbol{\theta}_0$ be some initial choice for $\boldsymbol{\theta}$ then the
 217 algorithm is as follows:

FOR $i = 1$ to N

- 1 Given current state $\boldsymbol{\theta}_i$ propose a new state $\boldsymbol{\theta}^*$ using $q(\cdot|\boldsymbol{\theta}_i)$
- 2 Put $\alpha = \min\{1, (\pi(\boldsymbol{\theta}^*)q(\boldsymbol{\theta}_i|\boldsymbol{\theta}^*)) / (\pi(\boldsymbol{\theta}_i)q(\boldsymbol{\theta}^*|\boldsymbol{\theta}_i))\}$
- 3 Go to 4 with probability α , otherwise set $\boldsymbol{\theta}_{i+1} = \boldsymbol{\theta}_i$ and
 218 return to 1
- 4 Simulate data $D^* \sim f(\cdot|\boldsymbol{\theta}^*)$
- 5 If $\rho(S(D^*), S(D)) \leq \epsilon$ then set $\boldsymbol{\theta}_{i+1} = \boldsymbol{\theta}^*$, otherwise set
 $\boldsymbol{\theta}_{i+1} = \boldsymbol{\theta}_i$

END FOR

219 Unlike [13] we put the MCMC rejection step 3 before the ABC comparison
 220 step 5, to avoid unnecessarily running the simulation in step 4. Note that if
 221 we wish to use a non-uniform kernel in step 5 (see for example Sisson and
 222 Yan [23] §4.3: a non-uniform kernel allows us to assign weights to those $\boldsymbol{\theta}^*$
 223 we accept, depending on $\rho(S(D^*), S(D))$, with smaller distances giving larger
 224 weights) then we can no longer separate the MCMC rejection step and the
 225 ABC comparison step, which increases the simulation burden. Sisson and Yan
 226 argue that using a kernel with unbounded support can improve the mixing of
 227 the Markov chain, however we did not find this to be a problem. In particular,
 228 using a regression adjustment [4] allows some relaxation of the threshold ϵ , to
 229 increase the acceptance rate without deliteriously impacting the posterior.

230 Practically, if $\boldsymbol{\theta}_0$ has very low posterior probability then ABC-MCMC can
 231 fail to accept any new sample points. Previous authors have suggested using
 232 a separate ABC step (without MCMC) to find a $\boldsymbol{\theta}_0$ with large posterior prob-
 233 ability; we found that using Simulated Method of Moments (SMM) instead
 234 requires much less computation time. SMM is a variant of the Generalised
 235 Method of Moments (GMM) that uses Monte-Carlo estimates of moments,
 236 rather than analytic expressions (McFadden 1989 [14]). Thus, like ABC, using
 237 SMM we have much more freedom in the choice of moments used to fit the
 238 model to the data, and we found that it worked well using the same summary
 239 statistics S that we use for the ABC fitting.

240 Following Wheeler et al. [26], for the CIN model the velocity \mathbf{v} , eccentricity
 241 e and orientation ω were all estimated using temporal and spatial autocovari-
 242 ance estimates, and then fixed. For the CIN-1 and CIN-2 models we used our

243 estimate of e for μ_e but also need to estimate σ_e^2 . To do this we divided the
 244 study region spatially into four equal parts, then estimated the eccentricity
 245 for each part at each time point, giving four time-series of estimates for μ_e .
 246 Treating each series as an AR(1) process with mean μ_e , we can correct for the
 247 autocorrelation to get the usual moment-based estimate for σ_e^2 .

248 The remaining parameters are all estimated using ABC. It is possible to
 249 include \mathbf{v} , e and ω in the ABC fitting rather than estimate them separately,
 250 however we found that doing so had no appreciable impact on the fit of the
 251 other parameters while it did increase the time required to run the ABC
 252 procedure.

253 We used the same set of 23 summary statistics for the CIN, CIN-1, and
 254 CIN-2 models:

- 255 – The overall mean and standard deviation of rainfall, taken over all pixels
 256 and all times.
- 257 – The spatial-temporal auto-correlation, with lags of (x, y, t) , where x and y
 258 are measured in pixels and t is in units of 6-minutes. We take $t = 0$, $x \in$
 259 $\{-1, 0, 1\}$, $y \in \{-1, 0, 1\}$, and $t = 1$, $x \in \{-1, 0, 1\} + v_x$, $y \in \{-1, 0, 1\} + v_y$.
 260 Here v_x and v_y are the velocity components, in units of pixels per 6-minutes.
 261 Note that the lag $(0, 0, 0)$ auto-correlation is just the variance and so has
 262 already been included.
- 263 – The probability of an arbitrary pixel and time being dry.
- 264 – The ratio of dry/wet area and mean and standard deviation of wet area,
 265 averaged over time.

266 For the distance function ρ we used a weighted sum of squares $\rho(S(D^*), S(D)) =$
 267 $\sum_i w_i (S^*(i) - S(i))^2$, where $S^*(i)$ and $S(i)$ are the i -th components of $S(D^*)$
 268 and $S(D)$ respectively. We found empirically that a good choice for w_i is to
 269 take it inversely proportional to the variance of $S^*(i)$ conditioned on using a θ
 270 with high posterior probability. Given that θ_0 was chosen using SMM to have
 271 maximal posterior probability, we used a separate sample of $S(D^*)$ given θ_0
 272 to calculate the w_i .

273 The choice of summary statistics S and distance metric ρ plays a large
 274 part in the performance of ABC. Ideally S should be sufficient, but certainly
 275 it should reflect those aspects of the real process considered most important.
 276 However choosing S too large reduces the efficiency of ABC, though this can
 277 be mitigated to some extent by using the approach of Beaumont et al. [4],
 278 which uses local linear regression to correct for bias in the posterior that can
 279 result from conditioning on $\rho(S(D^*), S(D)) \leq \epsilon$ instead of on $D^* = D$.

280 The remaining parameters were transformed to reduce dependence and
 281 skewness, and mapped to $(-\infty, \infty)$ (given as $\theta(1), \dots, \theta(9)$ and $\psi(1), \dots, \psi(11)$
 282 below). This makes it easier for the proposal chain to spend its time in regions
 283 of high posterior probability. Vague normal priors are used for all the trans-
 284 formed parameters, and for the proposal chain we used a random walk with
 285 $N(0, 0.2^2 I)$ steps.

For the CIN and CIN-1 model our new ABC-parameters are

$$\begin{aligned}\theta(1) &= \log(\lambda_s \gamma_s^{-1}), & \theta(2) &= \log(\lambda_s \gamma_s), \\ \theta(3) &= \log(\lambda_c \gamma_c^{-1}), & \theta(4) &= \log(\lambda_c \gamma_c), \\ \theta(5) &= \log(\mu_X \mu_A), & \theta(6) &= \log(\mu_X \mu_A^{-1}), \\ \theta(7) &= \log(\mu_{1/d_c}), & \theta(8) &= \log(\mu_{1/d_s}), \\ \theta(9) &= \log(CV_{1/d_s}).\end{aligned}$$

For the CIN-2 model we replace parameters μ_{1/d_c} and μ_A by μ_{d_c} and $\sigma_{d_c}^2$, and gain parameters σ_X^2 and ρ_{X,d_c} .

$$\begin{aligned}\psi(1) &= \log(\lambda_s \gamma_s^{-1}), & \psi(2) &= \log(\lambda_s \gamma_s), \\ \psi(3) &= \log(\lambda_c \gamma_c^{-1}), & \psi(4) &= \log(\lambda_c \gamma_c), \\ \psi(5) &= \log(\mu_X), & \psi(6) &= \log(1/\sigma_X^2), \\ \psi(7) &= \log(\mu_{d_c}), & \psi(8) &= \log(1/\sigma_{d_c}^2), \\ \psi(9) &= \log\left(\frac{\rho_{X,d_c} + 1}{1 - \rho_{X,d_c}}\right), & \psi(10) &= \log(\mu_{1/d_s}), \\ \psi(11) &= \log(CV_{1/d_s}).\end{aligned}$$

286 Comparison of Fitted Models

287 Using the spatial autocorrelation function we estimated $\mathbf{v} = (v_x, v_y) = (0.10, 29.9)$,
288 $e = \mu_e = 0.86$, $\sigma_e^2 = 0.04$ and $\omega = 39^\circ$.

289 In the Appendix Figures 9–11 plot the posterior sample traces for models
290 CIN, CIN-1 and CIN-2. In each case the chains appear stationary and exhibit
291 good mixing.

292 For the CIN model using a threshold of $\epsilon = 10$ the overall acceptance
293 rate was approximately 4.1%. Increasing ϵ improves the acceptance rate and
294 the degree of mixing, at the expense of reduced accuracy for the posterior
295 approximation. For the CIN-1 and CIN-2 models the acceptance rates were
296 approximately 5% and 11% respectively, using thresholds of $\epsilon = 14$ and 8. For
297 ABC-MCMC rather than the acceptance rate—which is commonly reported
298 for vanilla ABC sampling—a better measure of sampling efficiency is the “ef-
299 fective sample rate” for each parameter, which combines the efficiency of the
300 MCMC sampling and the ABC rejection step and is given by the effective
301 sample size for the sampling chain divided by the number of simulations re-
302 quired to produce them. For the CIN, the effective sample rate varied from
303 0.002 to 0.004 depending on the parameter. For the CIN1 and CIN2 models
304 the effective sample rate varied from 0.001 to 0.003 and from 0.001 to 0.005
305 respectively.

306 Posterior plots for models CIN, CIN-1 and CIN-2 are given in Figures 5–7.
307 In all three cases we get nice peaks on our posteriors. Posterior summaries

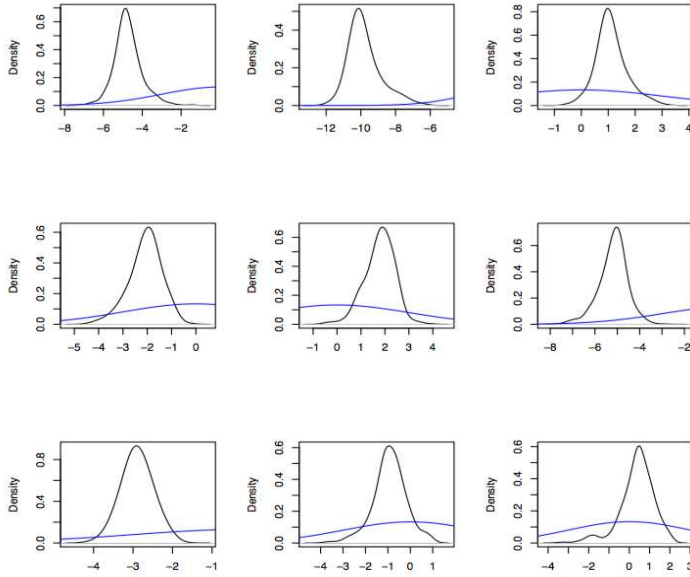


Fig. 5: CIN model: posteriors for $\theta(i), i = 1, 2, \dots, 9$. Priors are given by the dashed lines.

308 for the original (untransformed) parameters are given in Tables 1–3 in the
 309 Appendix.

310 To compare the performance of our three models we use posterior predictive
 311 probabilities to judge how close each model is to the original data, as measured
 312 by our distance ρ . That is, we compare for each model the distribution of
 313 $\rho(S(D^*), S(D))$ where D is the original data and D^* is generated by the model
 314 when θ is distributed according to the posterior. We can sample from this
 315 distribution by sampling θ from the posterior, generating D^* from θ and the
 316 model, and then calculating $\rho(S(D^*), S(D))$. We can then estimate the c.d.f.
 317 of $\rho(S(D^*), S(D))$ using the e.d.f. of a suitably large sample.

318 Figure 8 plots the estimated c.d.f. of the posterior for $\rho(S(D^*), S(D))$ under
 319 models CIN and CIN-1. We see that the CIN-1 model gives a better
 320 fit than the CIN model, that is, it is more likely to produce data close to our
 321 observation. The CIN-2 model does not give an improved fit, however it does
 322 show moderate evidence of negative correlation between cell intensity and
 323 diameter: the posterior mean for ρ_{X,d_c} is -0.69 with a 95% credible interval of
 324 $(-0.93, 0.10)$. We discuss the implications of this in the Conclusions section.

325 We can also construct posterior predictive distributions for $(S^*(i) - S(i))^2$.
 326 That is, we can compare the fit of each model as measured by individual
 327 components of the summary statistic S . They are given for the CIN and CIN-
 328 1 models in Figures 12 and 13 in the Appendix. Generally the CIN-1 model

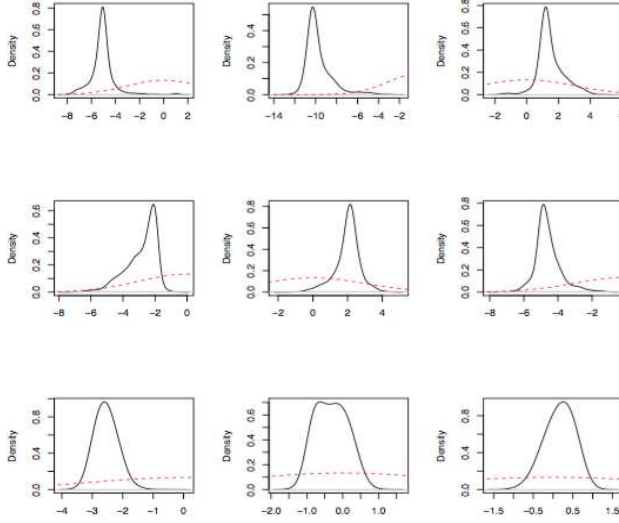


Fig. 6: CIN-1 model: posteriors for $\theta(i)$, $i = 1, 2, \dots, 9$. Priors are given by the dashed lines.

329 performs better than the CIN model, though not uniformly, but without any
 330 obvious pattern to the exceptions.

331 4 Conclusions

332 By using Approximate Bayesian Computation (ABC) we have been able to
 333 fit extensions of the spatial-temporal model of Cox, Isham and Northrop [7,
 334 15] (CIN model), allowing for more realistic rainfall intensity gradients and
 335 correlation between the intensity and size of localised rain cells. Using rainfall
 336 radar data for a rainfall event in Melbourne, Australian, and looking at the
 337 posterior predictive distribution of the distance between the observed and
 338 simulated data, we showed that the CIN-1 model gave a better fit than the
 339 CIN model. We also demonstrated moderate evidence for negative correlation
 340 between the intensity and size (diameter) of rain cells.

341 ABC is a very flexible methodology, and the approach demonstrated here
 342 could be easily applied to further generalisations of the CIN model. When in-
 343 troducing correlation between the cell intensity X and cell diameter d_c we used
 344 a multivariate lognormal distribution as this was a parsimonious way to do so,
 345 however it appears that while there is moderate evidence that the correlation
 346 is non-zero, qualitatively the lognormal marginals did a poor job of matching
 347 observed cell diameters, producing too many small cells. This suggests that we
 348 could improve the model further by using a copula to capture the dependence

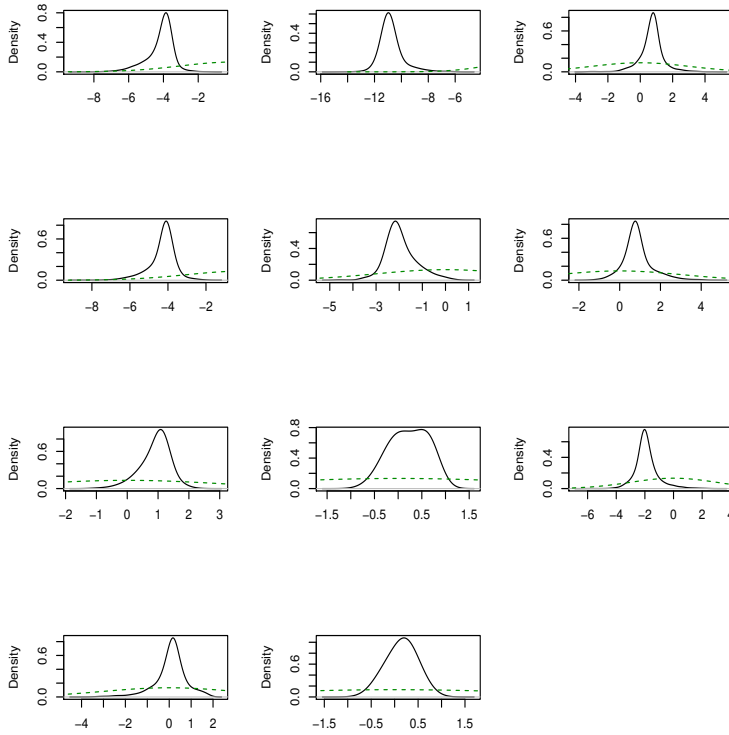


Fig. 7: CIN-2 model: posteriors for $\psi(i)$, $i = 1, 2, \dots, 11$. Priors are given by the dashed lines.

349 between X and d_c and experimenting with marginals other than the lognormal
 350 (the CIN and CIN-1 models use the exponential and gamma distribution for
 351 X and d_c respectively). A further extension would be to parametrise the cell
 352 intensity profile illustrated in Figure 4 to interpolate between the two models

353 More generally, by considering different components of the distance be-
 354 tween observed and simulated data we can see where one model outperforms
 355 another, which has the potential to inform future efforts at model refinement.
 356 Moreover additional components can be added to the summary S to focus on
 357 specific aspects of the model. For example if the maximum rainfall intensity
 358 produced by the model was considered particularly important, then this could
 359 be included in S and hence targeted when fitting the model.

360 Finally we note that from a technical point of view we showed that ABC-
 361 MCMC could be improved by separating the ABC and MCMC rejection steps
 362 and by using the Simulated Method of Moments (SMM) to initialise the pro-
 363 posal chain.

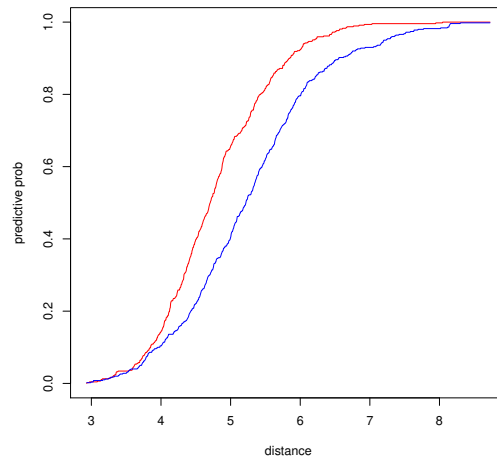


Fig. 8: Posterior distribution of $\rho(S(D^*), S(D))$ for the CIN model (blue) and CIN-1 model (red). The CIN-1 model is more likely to produce simulations D^* close to D , as measured by ρ , that is, it gives a better fit than the CIN model.

364 **Acknowledgements** Datasets for this research are available from the Australian Bureau of
365 Meteorology, GPO Box 1289, Melbourne VIC 3001. [http://www.bom.gov.au/climate/data-](http://www.bom.gov.au/climate/data-services/data-requests.shtml)
366 [services/data-requests.shtml](http://www.bom.gov.au/climate/data-services/data-requests.shtml). The Bureau charges according to the Australian Government
367 Cost Recovery Guidelines.

368 **Appendix**

369 Here we provide additional details of the model comparisons discussed in Sec-
 370 tion 3.

371 Figures 9–11 plot the posterior sample traces for models CIN, CIN-1 and
 372 CIN-2. In each case the chains appear stationary and exhibit good mixing.

373 Tables 1–3 give posterior summaries for the parameters of the CIN, CIN-1
 374 and CIN-2 models. We notice that for the CIN-2 model some credible intervals
 375 are wider than the CIN model and the CIN-1 model estimations, particularly
 376 mean storm duration γ_s^{-1} , mean cell duration γ_c^{-1} .

377 Figures 12 and 13 give posterior predictive distributions for $(S^*(i) - S(i))^2$,
 378 for the CIN and CIN-1 models. That is, we can compare the fit of each model as
 379 measured by individual components of the summary statistic S . Generally the
 380 CIN-1 model performs better, though not uniformly, but without any obvious
 381 pattern to the exceptions.

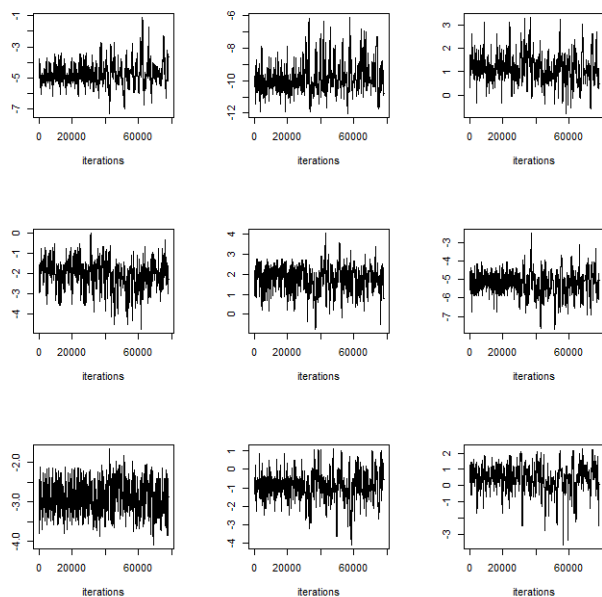


Fig. 9: ABC-MCMC fitting for CIN model: posterior chains for $\theta(i)$, $i = 1, 2, \dots, 9$.

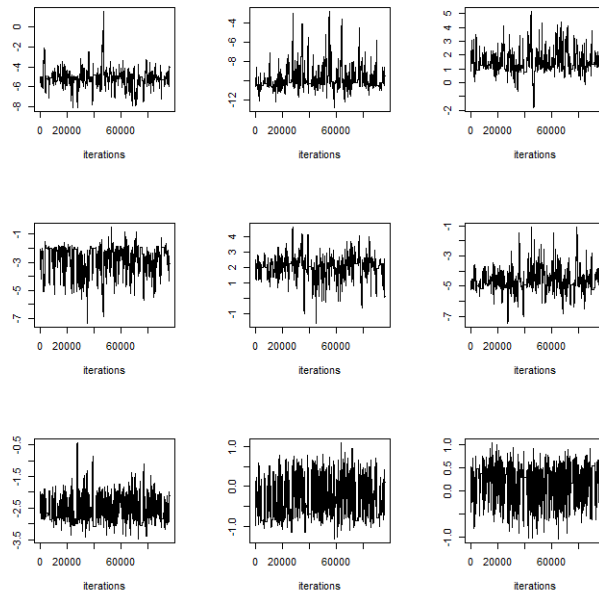


Fig. 10: ABC-MCMC fitting for CIN-1 model: posterior chains for $\theta(i)$, $i = 1, 2, \dots, 9$.

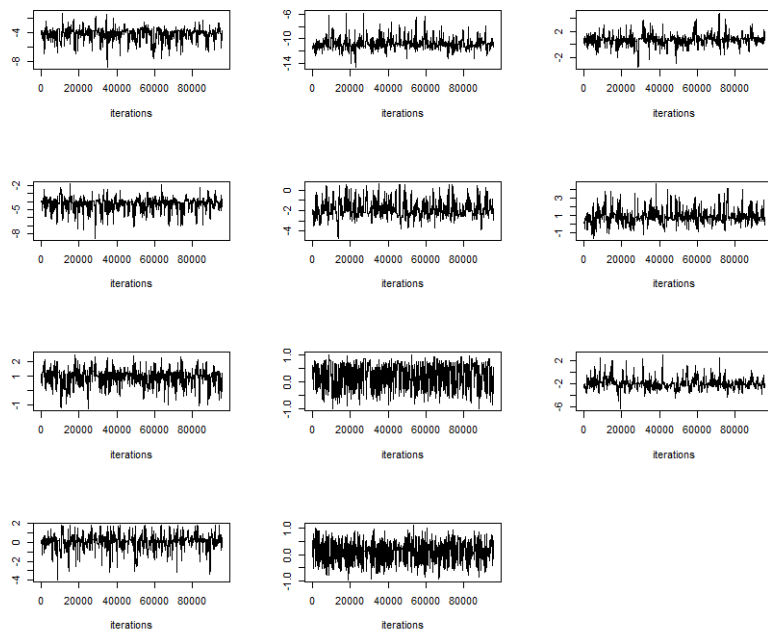


Fig. 11: ABC-MCMC fitting for CIN-2 model: posterior chains for $\psi(i), i = 1, 2, \dots, 11$.

Parameter	Mean	Median	95 % Credible Interval
λ_s	0.0008	0.0006	(0.0003, 0.0026)
γ_s^{-1}	14.8159	13.2333	(2.9086, 38.5852)
λ_c	0.6968	0.6201	(0.2321, 1.7451)
γ_c^{-1}	5.3733	4.6462	(2.6768, 13.1802)
μ_1/d_s	0.5199	0.4006	(0.0738, 1.8749)
CV_1/d_s	1.9438	1.5953	(0.1467, 6.0694)
μ_X	0.1946	0.1917	(0.0792, 0.3332)
μ_A	37.2997	32.6773	(11.8394, 93.7327)
μ_1/d_c	0.0595	0.0548	(0.0255, 0.1211)

Table 1: Posterior estimates of the ABC-parameters for the CIN model.

Parameter	Mean	Median	95 % Credible Interval
λ_s	0.0008	0.0005	(0.0002 0.0036)
γ_s^{-1}	12.7340	12.3910	(1.0938 38.4967)
λ_c	0.6166	0.5722	(0.1171, 1.8787)
γ_c^{-1}	10.7880	7.6703	(4.0369, 35.9604)
μ_1/d_s	0.8022	0.7224	(0.3761, 1.6064)
CV_1/d_s	1.2535	1.2105	(0.5601, 2.1132)
μ_X	0.2850	0.2731	(0.1508, 0.4848)
μ_A	33.0017	31.5407	(4.6533, 92.1609)
μ_1/d_c	0.0840	0.0771	(0.0441, 0.1617)

Table 2: Posterior estimates of the ABC-parameters for the CIN-1 model.

Parameter	Mean	Median	95% Credible Interval
λ_s	0.0006	0.0006	(0.0002, 0.00150)
γ_s^{-1}	31.797	32.462	(4.4944, 64.524)
λ_c	0.1887	0.1801	(0.0457, 0.4429)
γ_c^{-1}	13.883	11.407	(5.6338, 42.133)
μ_1/d_s	1.3331	1.1647	(0.1671, 4.3280)
CV_1/d_s	1.2102	1.1901	(0.6291, 1.9917)
μ_X	0.1882	0.1258	(0.0426, 0.7603)
σ_X^2	0.5235	0.4519	(0.0671, 1.5503)
μ_{d_c}	2.7478	2.7523	(0.7829, 5.6306)
$\sigma_{d_c}^2$	0.8602	0.7859	(0.4335, 1.7103)
ρ_{X,d_c}	-0.6906	-0.7564	(-0.9327, 0.0996)

Table 3: Posterior estimates of the ABC-parameters for the CIN-2 model.

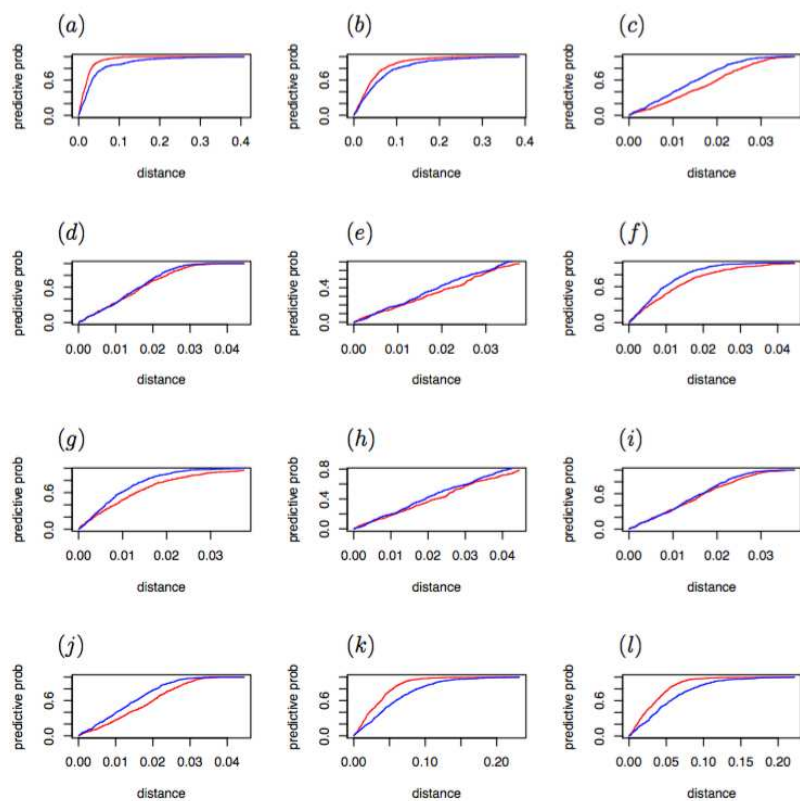


Fig. 12: Predictive probability for the CIN model (blue line) and CIN-1 model (red line). Plots (a) and (b) are for mean and standard deviation summaries. Plots (c) to (j) are spatial correlations $\rho(-1, -1, 0)$, $\rho(-1, 0, 0)$, $\rho(1, 1, 0)$, $\rho(0, -1, 0)$, $\rho(0, 1, 0)$, $\rho(1, -1, 0)$, $\rho(1, 0, 0)$, and $\rho(1, 1, 0)$. Plots (k) and (l) are of $\rho(-1 + v_x, -1 + v_y, 1)$, and $\rho(-1 + v_x, 0 + v_y, 1)$.

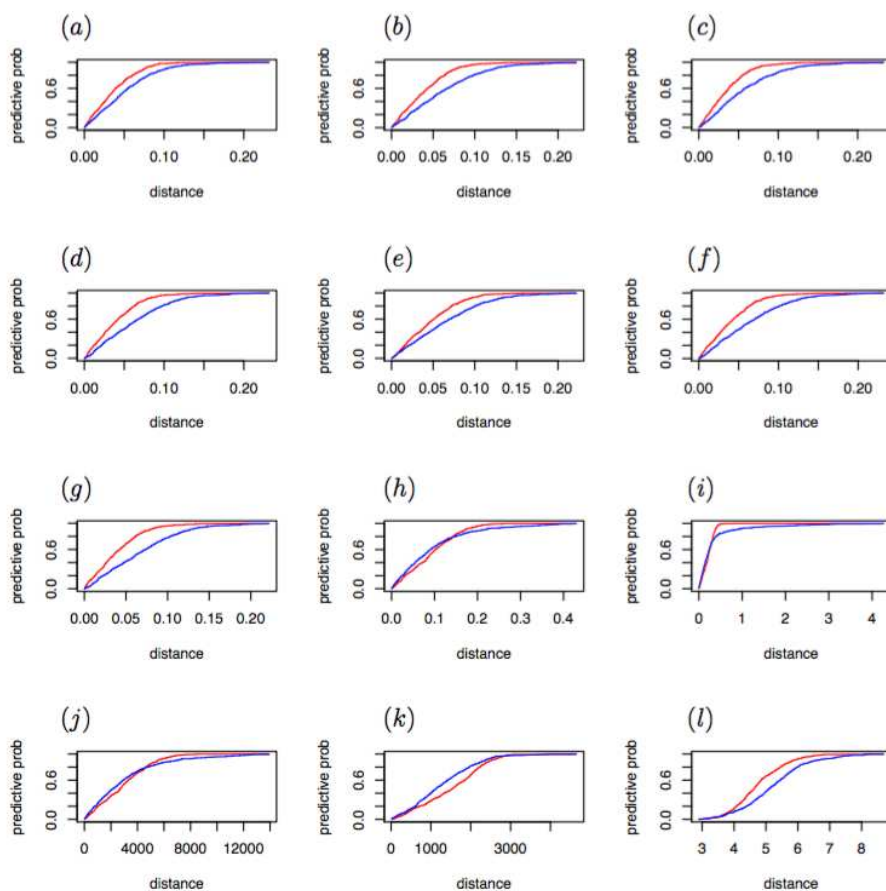


Fig. 13: Predictive probability for the CIN model (blue line) and CIN-1 model (red line). Plots (a) to (g) are of spatial autocorrelations $\rho(-1 + v_x, 1 + v_y, 1)$, $\rho(0 + v_x, -1 + v_y, 1)$, $\rho(0 + v_x, 0 + v_y, 1)$, $\rho(0 + v_x, 1 + v_y, 1)$, $\rho(1, +v_x, -1 + v_y, 1)$, $\rho(1, +v_x, 0 + v_y, 1)$, and $\rho(1, +v_x, 1 + v_y, 1)$. Plots (h) and (i) are of dry probability of an arbitrary pixel and dry and wet area ratio. Plots (j) and (k) are of mean wet area over time and standard deviation of wet area over time. Plot (l) is of total distance from all summaries.

382 References

- 383 1. Allard, D., Ailliot, P., Monbet, V., Naveau, P.: Stochastic weather generators: an
 384 overview of weather type models. *Journal de la Société Française de Statistique* **156**(1),
 385 101–113 (2015)
- 386 2. Aryal, N.R.: Stochastic spatial-temporal models for rainfall processes. Ph.D. thesis,
 387 School of Mathematics and Statistics, The University of Melbourne (2018)

- 388 3. Aryal, N.R., Jones, O.D.: Fitting the Bartlett-Lewis rainfall model using Approximate
389 Bayesian Computation. *Mathematics and Computers in Simulation* **175**, 153–163 (2020)
- 390 4. Beaumont, M.A., Zhang, W., Balding, D.J.: Approximate Bayesian Computation in
391 population genetics. *Genetics* **162**(4), 2025–2035 (2002)
- 392 5. Benoit, L., Allard, D., Mariethoz, G.: Stochastic rainfall modeling at sub-kilometer
393 scale. *Water Resources Research* **54**(6), 4108–4130 (2018)
- 394 6. Chandler, R., Isham, V., Northrop, P., Wheeler, H., Onof, C., Leith, N.: Uncertainty in
395 rainfall inputs. *Applied Uncertainty Analysis for Flood Risk Management*, edited by:
396 Beven, KJ and Hall, JW, Imperial College Press: London pp. 101–152 (2014)
- 397 7. Cox, D.R., Isham, V.: A simple spatial-temporal model of rainfall. *Proceedings of the*
398 *Royal Society of London A, Mathematical and Physical Sciences* **415**(1849), 317–328
399 (1988)
- 400 8. Gourieroux, C., Monfort, A.: Simulation-based inference. *J. Econometrics* **59**, 5–33
401 (1993)
- 402 9. Jones, O.D.: Modelling electricity power cuts in the UK. In: A. Stacey, B. Blyth, J. Shep-
403 herd, A.J. Roberts (eds.) *Proceedings of the 7th Biennial Engineering Mathematics and*
404 *Applications Conference, EMAC-2005, ANZIAM J.*, vol. 47, pp. C603–C620 (2007)
- 405 10. Jones, O.D., Nyman, P., Sheridan, G.J.: Modelling the effects of fire and rainfall regimes
406 on extreme erosion events in forested landscapes. *Stochastic Environmental Research*
407 *and Risk Assessment* **28**(8), 2015–2025 (2014)
- 408 11. Kaczmarek, J., Isham, V., Onof, C.: Point process models for fine-resolution rainfall.
409 *Hydrological Sciences Journal* **59**(11), 1972–1991 (2014)
- 410 12. Leclerc, G., Schaake, J.: Derivation of hydrologic frequency curves. *Tech. Rep. 142*,
411 *Mass. Inst. of Technol., Cambridge, MA, USA* (1972)
- 412 13. Marjoram, P., Molitor, J., Plagnol, V., Tavaré, S.: Markov chain monte carlo without
413 likelihoods. *Proceedings of the National Academy of Sciences* **100**(26), 15324–15328
414 (2003)
- 415 14. McFadden, D.: A method of simulated moments for estimation of discrete response
416 models without numerical integration. *Econometrica* **57**(5), 995–1026 (1989)
- 417 15. Northrop, P.: A clustered spatial-temporal model of rainfall. *Proceedings of the*
418 *Royal Society of London. Series A: Mathematical, Physical and Engineering Sciences*
419 **454**(1975), 1875–1888 (1998)
- 420 16. Onof, C., Chandler, R., Kakou, A., Northrop, P., Wheeler, H., Isham, V.: Rainfall
421 modelling using poisson-cluster processes: a review of developments. *Stochastic Envi-*
422 *ronmental Research and Risk Assessment* **14**(6), 384–411 (2000)
- 423 17. Park, J., Cross, D., Onof, C., Chen, Y., Kim, D.: A simple scheme to adjust poisson cluster
424 rectangular pulse rainfall models for improved performance at sub-hourly timescales.
425 *Journal of Hydrology* **598**, 126296 (2021)
- 426 18. Paschalis, A., Molnar, P., Fatichi, S., Burlando, P.: A stochastic model for high-
427 resolution space-time precipitation simulation. *Water Resources Research* **49**(12), 8400–
428 8417 (2013)
- 429 19. Peleg, N., Fatichi, S., Paschalis, A., Molnar, P., Burlando, P.: An advanced stochas-
430 tic weather generator for simulating 2-d high-resolution climate variables. *Journal of*
431 *Advances in Modeling Earth Systems* **9**(3), 1595–1627 (2017)
- 432 20. Pritchard, J.K., Seielstad, M.T., Perez-Lezaun, A., Feldman, M.W.: Population growth
433 of human y chromosomes: a study of y chromosome microsatellites. *Molecular biology*
434 *and evolution* **16**(12), 1791–1798 (1999)
- 435 21. Rodriguez-Iturbe, I., Cox, D.R., Isham, V.: Some models for rainfall based on stochastic
436 point processes. *Proceedings of the Royal Society of London A, Mathematical and*
437 *Physical Sciences* **410**(1839), 269–288 (1987)
- 438 22. Segond, M.L., Wheeler, H.S., Onof, C.: The significance of spatial rainfall representation
439 for flood runoff estimation: a numerical evaluation based on the Lee catchment, UK.
440 *Journal of Hydrology* **347**(1-2), 116–131 (2007)
- 441 23. Sisson, S., Fan, Y.: ABC samplers. In: *Handbook of Approximate Bayesian Computa-*
442 *tion*, pp. 87–123. Chapman and Hall/CRC (2018)
- 443 24. Sisson, S.A., Fan, Y., Beaumont, M. (eds.): *Handbook of Approximate Bayesian Com-*
444 *putation. Handbooks of Modern Statistical Methods*. CRC Press (2018)

-
- 445 25. Wheater, H., Chandler, R., Onof, C., Isham, V., Bellone, E., Yang, C., Lekkas, D.,
446 Lourmas, G., Segond, M.L.: Spatial-temporal rainfall modelling for flood risk estimation.
447 *Stochastic Environmental Research and Risk Assessment* **19**(6), 403–416 (2005)
- 448 26. Wheater, H., Isham, V., Chandler, R., Onof, C., Stewart, E.: Improved methods for
449 national spatial-temporal rainfall and evaporation modelling for BSM. Tech. rep., Defra
450 (2006)
- 451 27. Wood, S.N.: Statistical inference for noisy nonlinear ecological dynamic systems. *Nature*
452 **466**(7310), 1102–1104 (2010)